Krypton atom and testing the limits of extreme-ultraviolet tunable-laser spectroscopy

T. Trickl,[1,*] A. H. Kung,[2] and Y. T. Lee[3]
[1]*Forschungszentrum Karlsruhe, Institut für Meteorologie und Klimaforschung (IMK-IFU), Kreuzeckbahnstrasse 19, D-82467 Garmisch-Partenkirchen, Germany*
[2]*Institute of Atomic and Molecular Sciences, Academia Sinica, P.O. Box 23-166, Taipei, Taiwan 10617, Republic of China*
[3]*Office of the President, Academia Sinica, Nankang, Taipei, Republic of China*
(Received 15 August 2006; published 2 February 2007)

Measurements of several transitions in krypton carried out with a high-resolution extreme ultraviolet (xuv) laser source in 1987 were recently reanalyzed. This analysis, based on simulating the Doppler-broadened line shape of the iodine reference lines with new, greatly improved iodine reference data, yielded an order-of-magnitude improvement in the agreement between several ^{86}Kr transition frequencies between 94.5 nm and 116.5 nm to $\pm 5\times10^{-9}$. The overall relative uncertainty is estimated to be $\pm 6\times10^{-9}$, which matches the best accuracies achieved in nanosecond short-wavelength experiments. The influence of frequency chirping in the pulsed dye amplifier chain was estimated to be rather low and to vary approximately between −7.1 MHz and +5.0 MHz for the three laser dyes used in this experiment. It is concluded that with an even more careful laser design the chirp-induced frequency shifts could be reduced to less than 1 MHz. Based on the analysis of the presumable chirp effects a correction for the ^{86}Kr atlas by Kaufman and Humphries −0.055 53 cm^{-1} is determined, which agrees with the result of a very recent two-photon experiment with frequency combs within just 0.000 46 cm^{-1} (14 MHz), i.e., well within the combined errors of the three data sources involved in the intercomparison.

DOI: 10.1103/PhysRevA.75.022501 PACS number(s): 32.30.−r, 32.10.Fn

I. INTRODUCTION

High-resolution spectroscopy of the krypton atom has become an important tool for analyzing the performance of state-of-the-art high-resolution extreme-ultraviolet (xuv) laser systems [1–4]. The reasons for this are the relatively heavy mass around 84 u, yielding a reduced Doppler width, the availability of a considerable number of spectral lines in the most convenient spectral range accessible by frequency tripling in gases, and, most importantly, the high mutual accuracy of the excited-state level positions of 0.0001 cm^{-1} (3 MHz) (Refs. [5,6]). Trickl *et al.*, when testing their xuv laser system, studied five transitions of the six natural isotopes of krypton with a spectral resolution of about 210 MHz and determined the transitions frequencies, hyperfine parameters of ^{83}Kr, isotope shifts, lifetimes, and information on the electronic coupling [1]. Despite the high resolution achieved the absolute calibration accuracy was limited to about 0.007 cm^{-1} due to using reference data from the iodine atlas by Gerstenkorn and Luc [7,8]. Due to a recent revision of the iodine spectral data in the wavelength range 571–655 nm to within ±2 MHz [9,10] Brandi *et al.* were able to improve the krypton level positions to an uncertainty specified as 0.0013 cm^{-1} [3]. This value was ascribed mostly to the uncertainty in the frequency shift generated in the dye amplifier although some correction was made.

The frequency chirp in pulsed dye amplifiers [11–16], which may result in frequency shifts of up to 100 MHz [3], is obviously the limiting factor in precision xuv measurements. It has been ascribed to refractive-index changes or the time dependence of the gain. Measurements of the temporal behavior of the time-dependent shift of the instantaneous output frequency by using heterodyne techniques has become mandatory in recent precise measurements with pulse-amplified continous dye lasers. Reinhard *et al.* and Eikema *et al.* describe an experimental strategy of compensating the chirp with an electro-optic modulator [15,16]. The modulator creates an "antichirp" of the continuous seed beam that cancels the chirp of the amplifier system. This method has been successfully applied in precision measurements of the 58-nm transition of the helium atom [16], which was determined with a relative uncertainty of 8.8×10^{-9}. In earlier work the influence of the chirp had been reduced by filtering the pulsed radiation with a confocal etalon locked to the frequency of the continuous seed laser [17,18]. Another solution is the preparation of dye mixtures that shift the wavelength for which no chirp-induced offset exists to the spectral region of interest [19].

An overview of the specifications of some pulse-amplified continuous lasers applied in precision short-wavelength spectroscopy is given in Table I. The table lists type and pulse energy of the pump laser, the pump beam configuration (longitudinal or transverse), the output pulse length, and energy of the respective dye laser as well as the accuracy obtained and the magnitude of the chirp-induced frequency shift. The experiments have used different pump geometries, pump sources, and dye amplifiers, resulting in different implications for the chirp formation during the amplification. Without compensation frequency shifts were reported in all cases. In Ref. [17] no explicit value is given. The conclusion has been reached that side pumping the amplifier medium with a smooth pulse in a large volume should be advantageous although the experimental testing of this did not provide much evidence [13]. Longitudinal pumping was found to be important for providing an intensity sufficiently high to generate the tenth-harmonic radiation [16]. The higher output energies of 220 mJ were achieved at the expense of pro-

*Corresponding author. Email address: thomas.trickl@imk.fzk.de

TABLE I. Overview of the specifications of several high-accuracy vacuum ultraviolet (vuv) or xuv experiments with pulse-amplified continuous dye lasers; PL means: pump laser, PG: pump geometry (l—longitudinally pumped; s—side pumped; sf—side pumped and focused, sB—side pumped Bethune cell), RE: relative error. The frequency difference due to the chirp effects is given for the visible output; values in square brackets are estimated by us from a figure in the corresponding paper.

Authors	PL (E [mJ])	PG	E_{out} (mJ)	$\Delta t_{1/2}$ (ns)	BW (MHz)	RE	Chirp (MHz)
Wieman, Hänsch[11]	N_2 (13)	sf	5	7	[75]	n.a.	−17
Hildum *et al.*[17]	XeCl	sf	2.3	10	190	7.1×10^{-9}[a]	n.a.
Danzmann *et al.*[18,12]	XeCl (400)	s	70	24	30	8.7×10^{-9}	25–45[c]
Barr *et al.*[21]	Nd:YAG	n.a.	1.5	5	150–200	6.5×10^{-9}[a]	35–55
Gangop. *et al.*[13]	XeCl (150)	s/sf	9	<20	n.a.	n.a.	15–25
	Nd:YAG[b] (110)	sB	5	9.8	ca. 90 MHz	n.a	15–25
Eikema *et al.*[16]	Nd:YAG[b] (740)	1	220	6.5	90–95	8.8×10^{-9}	⩽30[c]

[a]Obtained from a comparison with the accurate value from Ref. [20].
[b]Injection seeded pump laser.
[c]Without chirp compensation.

nounced chirp problems, which are elegantly solved by the "antichirp" method mentioned above.

In the past the accurate calibration of the spectra was far from the resolution capibilities of the narrow-band pulsed laser sources if no special effort was made to reference the measurements to a secondary standard in the visible or infrared spectral region. Meanwhile, the iodine rovibronic data, which have been most frequently used for the frequency calibration of visible tunable lasers, have been thoroughly revised [22,23]. This analysis has resulted in a computer program which allows one to calculate the iodine spectrum between 515 and 820 nm with very high accuracy (IodineSpec4, commercially available from Toptica). The model reproduces any line between 526 and 667 nm with a 2σ uncertainty of ±3 MHz (between 760 and 820 nm even ±0.4 MHz), including the hyperfine structure, and provides the correct line envelopes as measured in Doppler-limited experiments. Given the high spectral resolution of our krypton spectra [1] we felt motivated by this new opportunity to revise our results. The high accuracy of the new frequencies also enables us to quantify the wavelength-dependent chirp effects in our laser system, which were not determined in the 1987 experiments, and, therefore, to address the respective criticism by Brandi *et al.* [3].

II. EXPERIMENTAL SETUP

The laser system was already described by us in detail in Ref. [24]. Here, we give a brief overview and focus on a few properties that are needed in the discussion of the results. The output of a continuous ring dye laser (Coherent Radiation, model 699-29, with an AUTOSCAN automatic tuning system), pumped by an argon ion laser, was amplified in three subsequent Bethune-type prism dye cells [25]. It is important to note that the cells, in contrast to those in many other systems, were side pumped, the pump beams for each of the cells being divided into four equal parts that pump the top, the bottom, and both sides of the cell. The main-amplifier cell (6 mm diameter) was as long as 60 mm. As a consequence, the pump intensity was just about 2% as com-

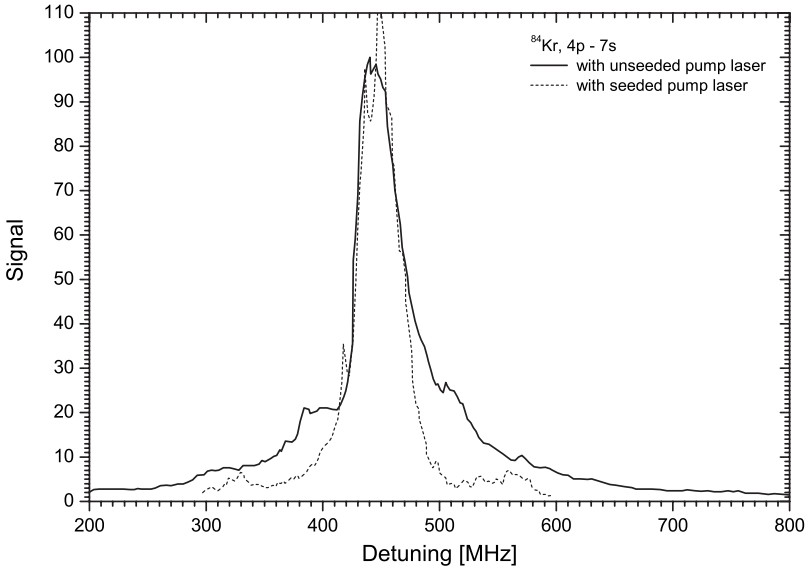

FIG. 1. Comparison of the ^{84}Kr $4p^6 \rightarrow 4p^5\,7s[^2P_{3/2}]$ $J=1$ line as excited with the pulse-amplifier dye laser pumped with an unseeded and a seeded doubled Nd:YAG laser; the slight asymmetry of the broader line is caused by signal averaging, the ringing superimposed on its profile is presumably caused by the detection electronics.

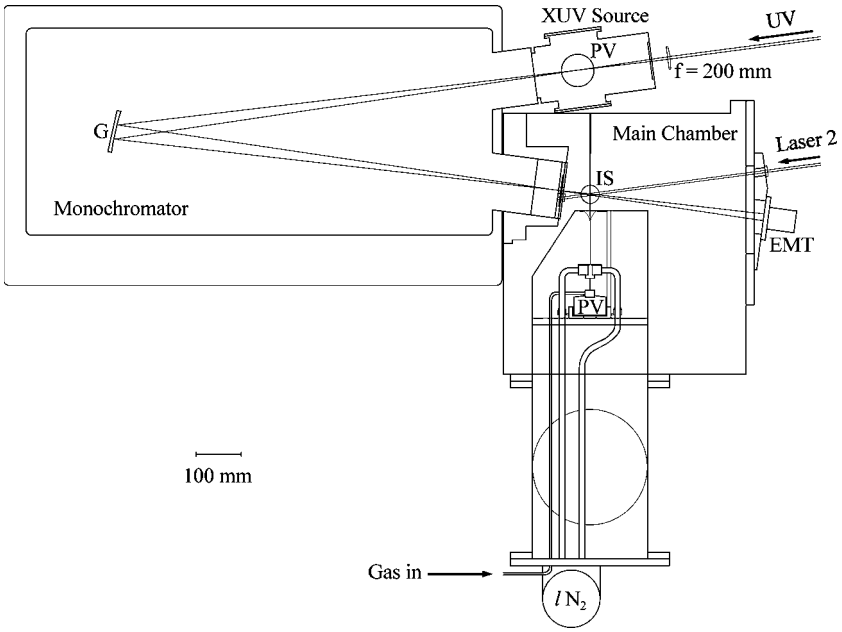

FIG. 2. Overview of the photoioization experiment: PV—pulsed valve, G—grating, IS—ion source, EMT—electron multiplier tube, *l*N2—liquid nitrogen reservoir (for our work with hydrogen dimers, not used in this experiment); the xuv source was pumped by a cryopump (about 1×10^{-3} mbar with the valve running), the monochromator (1×10^{-7} mbar) and the source chamber (about 2×10^{-5} mbar with the valve running) by diffusion pumps, and the main chamber (4×10^{-7} mbar) and the detector region (1×10^{-10} mbar) by turbomolecular pumps.

pared with longitudinal pumping. Due to the filled beam profile of the pump laser (Quantel International, model YG 595, repetition rate 10 Hz) the illumination was rather uniform along the cell and varied only next to the entrance and exit windows. The pump laser was injection seeded. The transition from an unseeded to a seeded version of the pump laser resulted in a substantial reduction of the wings of the emission line, which had resembled a Lorentzian rather than a Gaussian line prior to the change (Fig. 1, see also Ref. [13]).

The maximum output pulse energies for Rhodamine 590 (Rhodamine 6G) were between 120 and 130 mJ, achieved with a pump pulse energy of about 450 mJ. This high output is due to double passing the central amplifier, that yielded already almost 5 mJ. The amplified spontaneous emission (ASE) next to the maxima of the dye tuning curves was very low [26]. This was quite different in the regions of lower gain where the ASE could reach as much as 10% of the energy (and much more with the continuous seed beam off).

The pulse length Δt (full width at half maximum, FWHM) was 7.0 ns. The Fourier transform limit for pulses Gaussian in time is

$$\Delta\nu = \frac{2\ln 2}{\pi\Delta t}.$$

For 7.0 ns, a value $\Delta\nu$=67.9 MHz is calculated, which differs from the lower value of 32 MHz given by us earlier [24] based on electric fields rather than intensities. The 90-MHz bandwidth reported in Ref. [24] suggests some non-Gaussian behavior of the pulses. The bandwidth measurement was later repeated for 12 ns pulses [27]. A 52-MHz bandwidth was obtained which also exceeds the transform limit of 36.8 MHz. With higher pump pulse energies an output of even 170 mJ was demonstrated later on [52].

The photoionization apparatus is shown in Fig. 2. The frequency-doubled light from the dye laser was focused into a pulsed jet (pumped by a cryopump) for the generation of the xuv light. For the transitions discussed in this paper we used argon and xenon for the sum frequency mixing, selected from the tuning curves by Page *et al.* [28]. The pulsed valve was the final model described by Proch and Trickl and allowed a nozzle-limited flow for nozzle diameters up to 1.0 mm [29]. Due to achieving full flow through a 1.0-mm nozzle the conversion efficiencies could be improved with respect to earlier work, in particular in the case of argon as the tripling gas for which the first phase-matching maximum could be observed for the first time (Fig. 3). This had, in a preceding experiment, resulted in a greatly improved sensitivity for detecting hydrogen in the wavelength region around 101 nm [30], which was enhanced by almost another two decades with the laser system described here. In addition to the high conversion efficiency argon has a lower tendency for gas breakdown in the focus of the ultraviolet (UV) beam than the other gases used for the frequency conversion and is, therefore, the best choice for high-accuracy measurements (see Sec. III).

After the powerful UV (pulse energies up to 43 mJ) was removed in a 1-m monochromator (McPherson, model 225) the xuv beam entered the molecular-beam chamber and intersected the differentially pumped pulsed krypton beam at an angle of 97.5° necessitated by the basic frame set by the already existing main chamber and the monochromator [31,32]. The distance between the monochromator output and the atomic beam was, nevertheless, minimized by inserting a new, larger coupler between the two chambers. The xuv photons were detected with an electron multiplier mounted at the exit plate of the chamber which could be protected by a shutter when the monochromator was operated in zeroth order. The diffusion pump evacuating the monochromator was filled with Fomblin oil in order to avoid degrading of the grating.

The atomic beam source was a prealigned unit consisting of a second pulsed valve and the skimmer, which was inserted into the source chamber as a whole. In this way the uncertainty in the atomic beam pointing could be reduced to 0.03°. The nozzle diameter of the krypton source was

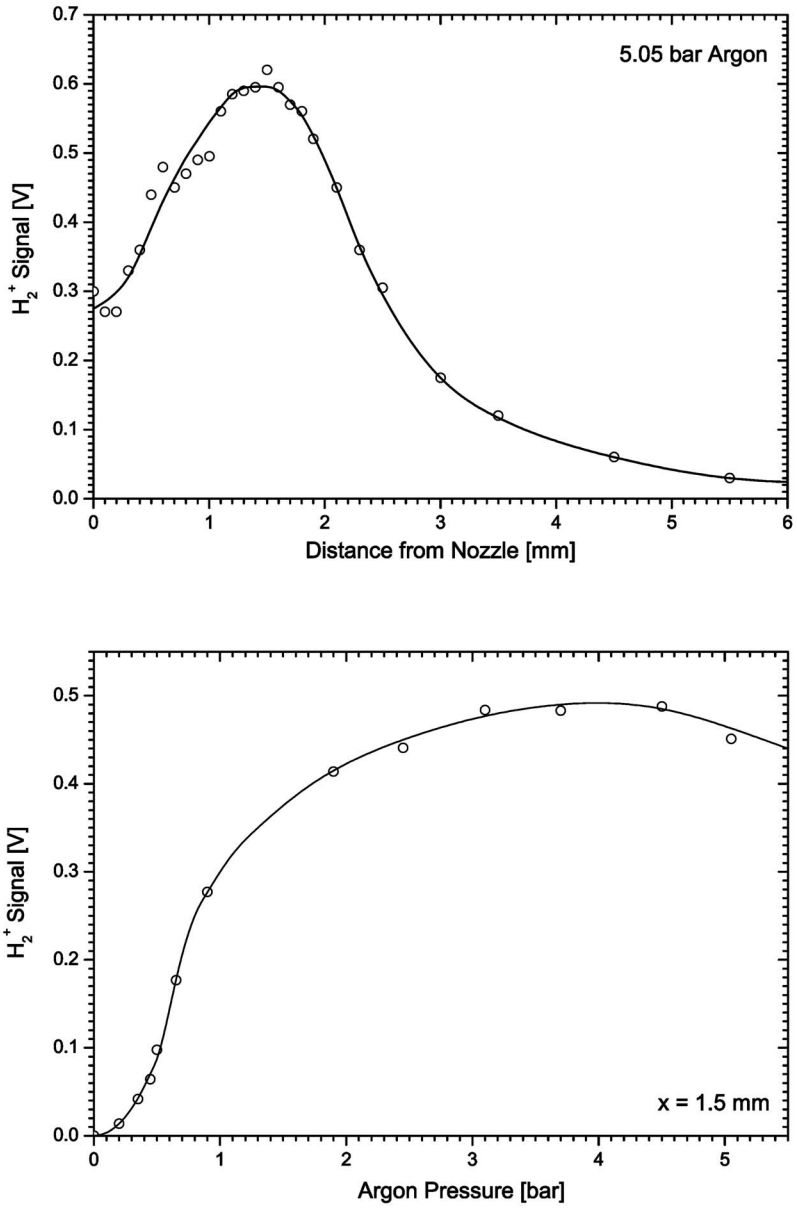

FIG. 3. Efficiency of the frequency tripling in argon at about 303 nm (upper panel) as a function of the distance of the UV focus from the nozzle (P=5.05 bar), (lower panel) as a function of pressure when focusing the UV beam to 1.5 mm downstream of the nozzle; the incident UV pulse energy was 6.5 mJ (from a frequency-doubled Quanta Ray PDL dye laser). The efficiency curve was obtained by measuring the hydrogen two-photon ionization signal for exciting the $X \rightarrow C$ (0,0) Q_1 line in H_2 as the first step.

0.2 mm, the skimmer diameter 1.0 mm, and the nozzle-skimmer distance 100 mm [chosen for our (still unpublished) photoionization work with hydrogen dimers in the wavelength range between 74 and 80 nm], which resulted in a low gas beam divergence and Doppler width, advantageous for the experiment described here. The skimmer was subsequently replaced by a larger one in order to achieve a better overlap of the gas and the xuv beam.

High backing pressure may result in collisions in the skimmer region. We had examined this in some detail when testing our source with hydrogen (for a shorter nozzle-skimmer distance of 19 mm) and had found a pronounced Doppler-broadened component for pressures above 1 bar. In order to avoid such problems we mostly limited the krypton pressure to values of 1 bar and less. In this way also the line broadening due to the very strong light absorption in the atomic beam for the shortest-lived transitions was reduced. A residual influence of collisions within the skimmer cannot be excluded. Indeed, quite a few spectra show small broadband contributions in some agreement with the expectation from the Doppler shifts derived for the skimmer cone angle.

The excited krypton atoms were ionized with a second laser [harmonic of Nd:YAG laser (Quanta Ray, model DCR 2A) or pulsed dye laser (Quanta Ray, model PDL)]. The wavelengths were selected to limit the excess energy during the ionization process (see Table I in Ref. [1]). In order to avoid power-induced line shifts the second laser was delayed in the case of the four transitions reanalyzed here [1]. The ionizing laser was sent into a beam dump covered by a quartz plate in order to avoid a potential formation of charged particles on the metallic surfaces of the chamber.

A crucial part of the experiment was the selection of the individual krypton isotopes, which could not be spectrally resolved. For the selection a 1-m time-of-flight mass spectrometer was developed. The ions were generated in a large volume limited by the 3.5-mm diameter of the xuv beam difficult to be focused in time for a sufficient mass resolution. Since a reflectron-type mass spectrometer [33–35] was

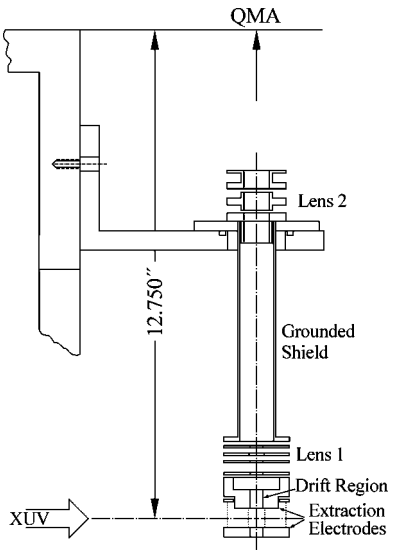

FIG. 4. Ion optics of the time-of-flight mass spectrometer (lowest section); QMA means quadrupole mass analyzer. The diameter of the entrance hole of QMA was about 4 mm.

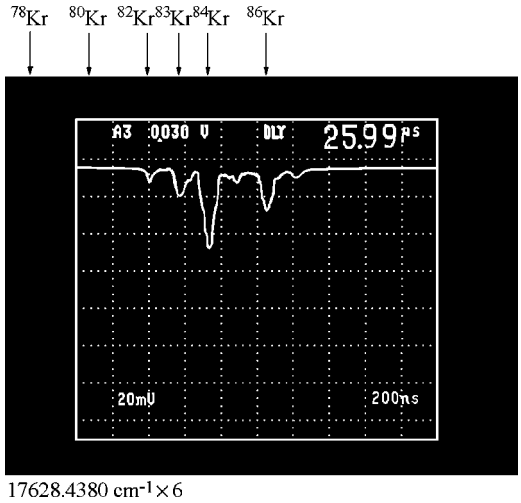

FIG. 5. Time-of-flight mass spectrum of Kr for a selected wavelength in the $4p^6 \rightarrow 4p^5\,7s[^2P_{3/2}]\ J=1$ transition; the wave number shown is that displayed by the CR 699-29 wave meter and is, therefore, not quantitative.

beyond the scope of this photoionization project, a different approach had to be found. The solution is based on the fact that the ions generated closer to the repelling anode are accelerated to slightly higher velocities than those further distant. After drifting in a field-free environment to a distance from the end of the first acceleration field equal to the distance between the two extraction electrodes (Fig. 4) the ions arrive at approximately the same time. Subsequently, the velocity distribution is compressed by strong acceleration [36], the overall acceleration voltage normally being about 1 kV. A mass resolution sufficiently high for the planned experiments with light or moderately heavy molecules was achieved. Above the main chamber the ions drifted through an optional quadrupole mass analyser (Extranuclear). At the top the ions were detected with a Daly detector [37] equipped with a Johnston electron multiplier. The detector region with its very high fields was electrostatically separated from the mass spectrometer by four apertures which were also used to optimize the signal.

In the case of krypton interference from abundant neighboring isotopes could not always be fully suppressed. In order to minimize this interference a considerable effort was spent on each measurement day to optimize the mass selection. Just a slight reduction of the UV beam diameter was possible by using an aperture since the outer part of the xuv radiation contained most of the intensity. However, the ring-shaped intensity distribution of the xuv beam and, in particular, the ionizing laser opened up another possibility to improve the mass resolution. Just the upper section of each ring was overlapped with the atomic beam in the center of the ion source. Figure 5 shows a mass spectrum obtained for the $4p^6 \rightarrow 4p^5\,7s[^2P_{3/2}]\ J=1$ transition, which demonstrates a reasonable resolution $[m(\Delta m)^{-1} \approx 660]$. Due to the small isotope shifts contributions from a total of four krypton isotopes are seen at the wavelength used in this case.

For high-accuracy calibration scans the overall voltage was reduced to below 100 V in order to avoid field-induced line shifts (see Sec. III). This slightly deteriorated the mass resolution and considerably reduced the ion transmittance. By using a low acceleration voltage the application of a delayed pulsed ion extraction as in our preceding N_2 photoionization study [38] could be avoided.

In the case of the ^{83}Kr precision scans we used the quadrupole mass analyzer for a better rejection of contributions of the close-by ^{82}Kr and ^{84}Kr isotopes. The operation of this mass analyzer implied a pronounced temporal stretching of the single-isotope peaks width thus scrambling the time-of-flight information. Since the transmittance of the mass spectrometer was zero for overall voltages below 60 V, the quadrupole analyzer could not be operated in its optimum ion-velocity range. As a consequence, the ^{83}Kr spectra still contained small contributions from the neighboring isotopes, in this case mostly ^{84}Kr due to its predominant abundance.

The entire optimization procedure, also implying a reduction of the UV power in the xuv source in order to avoid arc formation (see Sec. III), resulted in a signal loss by several orders of magnitude and frequently noisy spectra. The extraction of the hyperfine parameters was, therefore, in most cases based on averaging the results for many individual scans.

The laser frequency was monitored with a confocal etalon with a free spectral range (FSR) of 300 MHz and a single-fringe bandwidth of about 5 MHz (full width determined with ring laser: 6 MHz). The FSR was calibrated with iodine reference lines. This calibration verified a linear behavior of the fringe distances during the individual frequency scans although the FSR was found to vary from experiment to experiment. The linear performance means a constant or linearly varying temperature during a scan.

The iodine calibration scans were performed with the output of the continuous laser rather than with the pulse-amplified radiation although the bandwidth measurement with Rhodamine 590 had shown a +9 MHz offset of the overall output with respect to the ring-laser frequency. This was necessitated by a missing component. At the time of the

experiment a frequency shift of 9 MHz could be regarded as small in comparison with the ±30 MHz uncertainty expected for the calibration with the iodine reference spectrum.

The absolute frequency calibration was carried out for ^{83}Kr since the outer ($F=7/2$ and $F=11/2$) hyperfine components were not influenced by a spectral overlap with the background from other isotopes. The line positions of the other isotopes can be derived from the isotope shifts determined in independent measurements, carried out with two boxcar gates simultaneously set to the mass peaks of two isotopes.

The signals were processed with boxcar integrators (Stanford Research Systems, model SR250). They were averaged over just ten laser shots in order to limit the asymmetric spectral line broadening due to the exponential averaging (see Fig. 1). Averaging could not be completely avoided due to the strong fluctuations of the xuv intensity and the ion signal. The nonlinear influence of exponential averaging was carefully simulated for the bandwidth analyses in Sec. IV A, using the expressions provided by Stanford Research Systems.

III. CORRECTIONS AND ERROR CONSIDERATIONS

Apart from the frequency chirp already introduced in Sec. I there are a number of error sources that can lead to a modification of the results. We have tried to minimize carefully the influence of the different sources on our results.

Disregarding the chirp problem the data evaluation contains just a single correction, the compensation of the Doppler shift caused by the 97.5° angle between the xuv and the Kr beam. This shift depends only on the speed of the atomic beam, which can be accurately calculated for the known isotopic mixture [39]:

$$v_\infty = \sqrt{\frac{2kT\kappa}{m(\kappa-1)}},$$

with

$$m = \sum_{i=78}^{86} x_i m_i.$$

Using the isotopic relative abundances x_i as already used in Ref. [1] (^{78}Kr: 0.35%, ^{80}Kr: 2.27%, ^{82}Kr: 11.56%, ^{83}Kr: 11.55%, ^{84}Kr: 56.90%, ^{86}Kr: 17.37%), the adiabatic exponent $\kappa=5/3$ and an estimated beam source temperature $T=22.5(\pm2)$ °C (in agreement with the average of recent measurements kindly carried out for us) a speed of 382.77(±1.3) m s^{-1} and a frequency correction factor of 1.000 001 666 5(56) are obtained. The theoretical relative deviation from the maximum speed for distances exceeding 10 mm (50 times the nozzle diameter) is below 0.079% (Mach number $M>43.662$) [39]. It was experimentally shown that the adiabatic energy limit is reached for argon and helium atoms within less than 0.8% for Mach numbers of 20 and more [40]. For lower Mach numbers (but $M>2.5$) the adiabatic limit is even slightly exceeded, with a maximum deviation of 2.2% around $M=10$. Due to the square-root law the corresponding velocity increase is just 1.1%. The deviation under our conditions is very likely much lower and, thus, negligible in the error budget.

The divergence of the xuv beam emerging from the grating spectrometer, necessitated by the need for a small beam diameter in the atomic beam, yields a small angular asymmetry with respect to the molecular beam axis. The angular range was roughly ±0.9°. This yields a negligible shift of the line center by less than 0.3 MHz. The angle of the xuv beam is known to within ±0.02% and does not contríbute to the error budget. As described above, the molecular beam is carefully aligned and should contribute less than 0.4% to the uncertainty in the intersection angle.

As another potential source of error we identified the optical breakdown in the tripling gas. Spark formation in xenon was observed through the side window of the xuv source. In order to avoid potential Stark shifts due the high intensity we reduced the UV pulse energy to values clearly below the threshold for spark formation and/or reduced the gas pressure by slightly increasing the distance between nozzle and focus. Spark formation in argon was observed only at the highest available UV energies. We conclude that the results obtained with argon as the tripling gas are the most reliable ones. The correctness of our assumption of intensity-induced line shifts was verified by Eikema *et al.* [16]. They carefully examined the effect and found that even at their substantially higher intensity the shift of the tenth-harmonic frequency (used for their measurements of the $1\,^1S \rightarrow 2\,^1P$ transition of helium) can be minimized to levels of about 10 MHz (i.e., 1 MHz for the visible laser).

For most measurement series the isotope shifts for the even isotopes could be represented by a Bohr-type model to within typically ±15 MHz. In the case of ^{83}Kr the determination of the position of the central $F=9/2$ hyperfine component was sometimes slightly influenced by the contaminations in the mass spectrum, which were difficult to resolve in the case of the rather congested 6*s* and 7*s* spectra. As a result there is some small uncertainty about the *B* constant and, thus, also of the ^{83}Kr isotope shift with respect to ^{86}Kr. In order to determine the ^{86}Kr frequencies we took the frequency differences with respect to the positions of the outer ^{83}Kr hyperfine components wherever available.

The influence of the static ion-extraction field was determined for the transition to the $6s[^2P_{3/2}]$ $J=1$ state. A sensitivity of +8.91(12) MHz (100 V)$^{-1}$ with respect to the overall acceleration voltage of the ion beam was found (xuv wave number). Since the measurements and, in particular, the ^{83}Kr scans were carried out with voltages below 100 V we neglect this shift although it might be larger in the case of the 7*s* state.

The slopes of the Doppler-broadened iodine lines are sufficiently steep to allow one to determine the edges with a precision of the order of 1 MHz. In the absence of the original calibration scans no least-squares fitting procedure could be applied to adjust the krypton frequencies to the iodine reference spectrum. Instead, "centers of gravity" (see Ref. [8]) were calculated in order to make the procedure comparable to that used for the analysis of the measured spectra. The center of gravity of a single line was obtained by averaging the line centers derived for a sequence of equidistant signal levels.

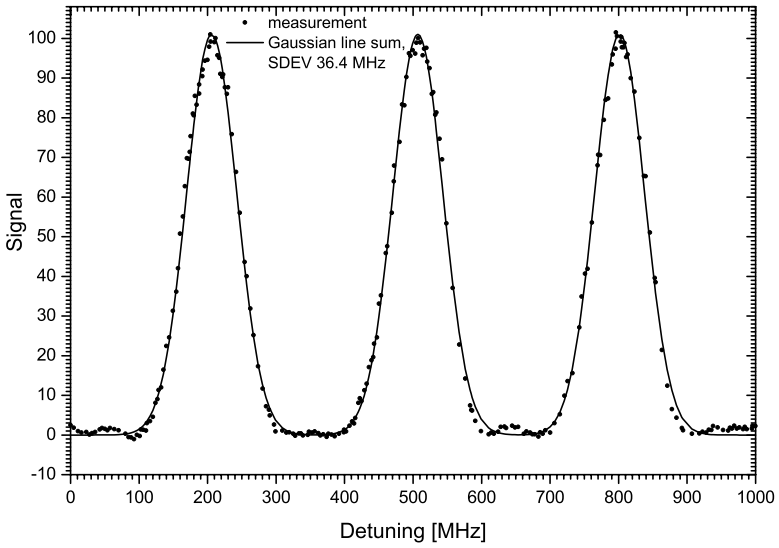

FIG. 6. Bandwidth determination with the 300-MHz-FSR confocal etalon; the fringes are nicely reproduced by Gaussian lines with a standard deviation of 36.4 MHz, corresponding to a full width at half maximum of 85.7 MHz.

The Doppler-broadened iodine spectrum in the vicinity of each krypton line was calculated for 25 °C with the IodineSpec4 program. The line-centering uncertainty achieved for most of the equidistant signal levels is about ±0.4 MHz, i.e., approximally equal to the uncertainty for the evaluation of the measured spectra. A much larger error is expected to originate in the possibly different treatment of strongly asymmetric lines deformed by an overlap with a second, smaller line. A comparison was not possible since the 1987 spectra no longer exist. In these cases, the choice of the position of the lower signal cutoff level for the center-of-gravity determination has a pronounced influence on the results. The error contribution from the unknown cutoff level was estimated by sensitivity studies.

Finally, frequency shifts caused by the pulsed amplification must be taken into consideration. During the bandwidth measurements we found a positive frequency shift of the pulsed dye-laser output with respect to the continuous seeder by roughly 9 MHz. This value is somewhat uncertain since a careful reanalysis of this measurement is not possible in the absence of the original data and notes. Motivated by the criticism in Ref. [3] concerning an insufficient analysis of the strongly wavelength-dependent shifts we discuss the influence of a potential frequency chirp in more detail in Sec. IV C. This analysis has become possible because of the greatly improved determination of the xuv transition frequencies described in Sec. IV B.

IV. RESULTS AND DISCUSSION

A. Laser Bandwidth

As the first step to characterize our laser system more carefully we reevaluated one of the bandwidth measurements. For this wavelength (presumably in the region around 570 nm where most of the early measurements were done) originally the +9 MHz frequency shift between the pulsed and the continuous output had been found. The result of the reanalysis is shown in Fig. 6 (an example different from that in Ref. [24] for which we cannot exclude the onset of detector saturation). Apart from some small deviations caused by an oscillating signal background the signal could be nicely approximated by a sum of three Gaussian curves with a half-signal width of 85.7(5) MHz. By subtracting the broadening of 3.0 MHz caused by averaging the signal with the boxcar averager for ten laser shots during the 10 MHz/s dye-laser scans and the contribution of the confocal etalon of 5 MHz we arrive at a bandwidth of the pulse-amplified system of 77.7(7) MHz. The Fourier transform limit for our 7.0-ns pulses, corrected for the 500-MHz oscilloscope bandwidth to 6.97 ns, is 63.3 MHz which is closer to the value obtained from the measurement than previously thought.

The measurement by Vrakking *et al.* for the 12-ns pulses (Sec. II) [27], if analogously corrected (the broadening is 4.0 MHz for the smaller bandwidth), yields a bandwidth of 43.0(11) MHz, very close to the respective transform limit for 11.98 ns of 36.8 MHz.

For the determination of the xuv bandwidth the $4p^6 \rightarrow 4p^5\,7s[^2P_{3/2}]\,J=1$ transition was preferred due to the long 130-ns lifetime. The result of the simulation of a ^{84}Kr measurement is shown in Fig. 7. A small contribution of neighboring isotopes and 3% of a broadened background (706 MHz FWHM) is accounted for. The strong narrow part of the line profiles was calculated as a Gaussian with 195(5) MHz FWHM. The envelope of the synthesized spectrum was numerically filtered by following the description in the boxcar instructions and assuming 10-shot averaging. For the calculation of the Kr Doppler width we assume that atoms leaving the nozzle next to its edge are not likely to cross the atomic-beam axis (justified by the result of the bandwidth calculation further below). This approximately yields a point source and leads to a $4p^6 \rightarrow 4p^5\,7s$ Doppler width of 40.1(80) MHz and a xuv bandwidth of 154.9 MHz. The bandwidth of the sixth harmonic of a pulse Gaussian in time is $\sqrt{6}$ times the fundamental bandwidth. From this, a dye-laser bandwidth of 63.2(39) MHz is calculated that is very close to the transform limit given above and indicates that the chirp for the $7s$ wavelength of 567 nm must be rather small, in some agreement with the results in Sec. IV C.

From these considerations we conclude that the chirp-induced frequency shift for our laser system at this wave-

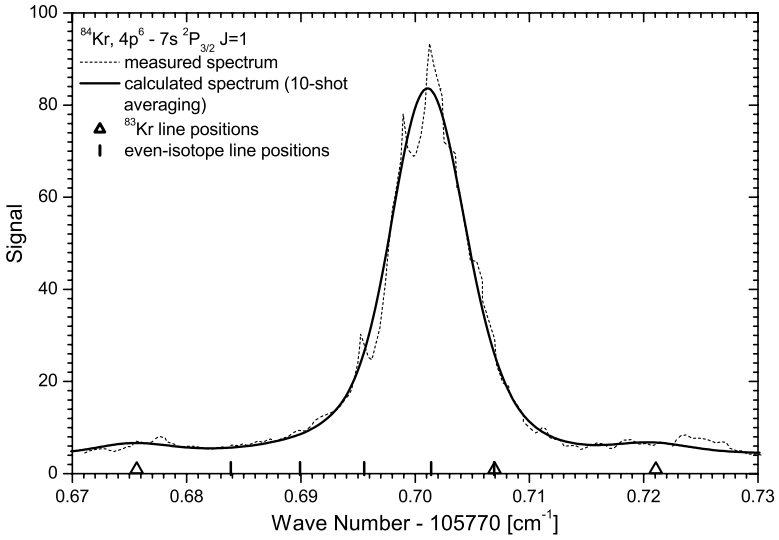

FIG. 7. Determination of the xuv bandwidth by an analysis of the ^{84}Kr $4p^6 \rightarrow 4p^5\ 7s[^2P_{3/2}]\ J=1$ line (see text).

length is rather limited and should, in the above cases, not significantly exceed half the bandwidth difference of 6.7 MHz for the 7-ns pulses (and 3.1 MHz for the 12-ns pulses at the respective wavelength). We cannot exclude that the sixth-harmonic generation "cleans" the pulse to some extent as suggested by the conversion of the xuv line width to a visible bandwidth. The narrow xuv bandwidth suggests that no significant frequency shift should have occurred during the sum frequency mixing process.

B. Revision of the krypton data

Four of the five transitions studied in Ref. [1] were revised, i.e., those for which a direct calibration in the visible spectral region existed: $4p^6 \rightarrow 4p^5\ 5s'[^2P_{1/2}]\ J=1$, $4p^5 6\,s'[^2P_{1/2}]\ J=1$, $4p^5\ 6s[^2P_{3/2}]\ J=1$, and $4p^5\ 7s[^2P_{3/2}]\ J=1$. First of all we realized that the wave number in Ref. [1] for the $4p^6 \rightarrow 4p^5\ 6s[^2P_{3/2}]\ J=1$ transition is wrong due to a mistake in copying a single digit of the visible ^{86}Kr wave number in our notes (16 649.003 148 cm^{-1} instead of 16 649.006 148 cm^{-1}). The corrected xuv wave number (99 894.0517 cm^1) is not far from the final value in this paper, which is explained by a very small deviation of the nearby iodine line 3970 in the iodine atlas [7,8] from its true position. We obtain a revised average correction for the data in Ref. [5] of −0.0619(61) cm^{-1} which now agrees with the value in Ref. [3], −0.0558(13) cm^{-1}, within the error limit.

Since the original spectra are no longer available, the revision of the data was based on copies of the rather explicit notes taken in 1987. However, these copies are not complete. They cover the entire analysis of the hyperfine structure and the isotope shifts, but many pages on the calibration measurements and the calibration spectra themselves are missing. The new calibration was achieved in two ways. For the two transitions for which a documentation of the fringe positions of the reference interferometer as well as the relative positions of the spectral lines with respect to these fringes existed ($4p^6 \rightarrow 5s'$ and $4p^6 \rightarrow 6s$) the calibration of the reference interference fringes and the krypton line positions could be completely revised. For the other two transitions ($4p^6 \rightarrow 6s'$ and $4p^6 \rightarrow 7s$) the relative positions of the krypton lines with respect to the adjacent two iodine lines (old frequencies) were calculated. The new Kr frequencies were then obtained by applying the fractions derived in this way to the difference of the revised I_2 line positions. Since the new calibration changes the effective free spectral range of the reference etalon for the respective measurement periods also the hyperfine parameters were carefully revised (see below).

The $4p^6 \rightarrow 6s$ transition could be particularly well recalibrated since the positions of the reference fringes next to the centers of even four iodine reference lines (3970 to 3973) were available. The conversion from the old iodine frequencies to the new ones resulted in a fit of the four fringes with a standard deviation of 1.5 MHz, reproducing the most important gravity center of line 3970 (which is very close to the Kr lines) to just within 0.26 MHz.

All calibration scans were carried out with ^{83}Kr because of the simultaneous interest in an evaluation of accurate hyperfine parameters and the low contamination of two of the three hyperfine components by the other isotopes. The uncertainty for the ^{83}Kr line center is rather low for the spectra with well-separated lines where also the residual contamination from neighboring isotopes did not influence the central $F=9/2$ hyperfine component. Since the conversion to ^{86}Kr contributes an error, the analysis of the isotope shifts was very carefully reexamined.

The results of the revision are listed in Table II together with the corresponding reference value by Kaufman and Humphries [5] to allow a comparison with our earlier work [1] and the publication by Brandi *et al.* [3]. The agreement with the results in Ref. [3] is highly satisfactory. The errors are given with and without the contribution from the iodine-based calibration. They do not include any assumption on the influence of the frequency chirp.

No interferometrically determined value is available for the $6s'$ state. Therefore, we looked for additional transitions from those listed in Ref. [5] to the $6s'$ state to calculate this level position. In order to minimize the error inferred by this indirect procedure we focused on transitions in the infrared. Table 1 given by Hernäng [41] contains four suitable lines, which are not included in Ref. [5]. The wave-number accuracy of this table is specified as 0.02 cm^{-1} at 1000 nm and

TABLE II. Revised Level Positions of ^{83}Kr and ^{86}Kr: the upper entry for each state corresponds to ^{86}Kr, the lower one to ^{83}Kr. The errors for Ref. [5] do not contain the relative contribution of the excited states. The error brackets in third column contain the error estimate without and with the uncertainty of the iodine centers of gravity. Potential systematic errors due to the laser system (which are quantified in Sec. IV C) are excluded. All values are given in cm^{-1}.

State	Harmonic	σ (cm^{-1})	σ [cm^{-1}] (Ref. [5])	Difference (cm^{-1})
$5s'[^2P_{1/2}]$ $J=1$	5th	85846.70642(35,52)	85846.7624(1)	0.05598(53)
		85846.70186(25,46)		
$6s'[^2P_{1/2}]$ $J=1$	6th	105146.32335(51,130)	105146.38568(707)*	0.06233(719)
		105146.31398(36,125)		
$6s[^2P_{3/2}]$ $J=1$	6th	99894.05300(49,64)	99894.1081(1)	0.05510(65)
		99894.04767(30,50)		
$7s[^2P_{3/2}]$ $J=1$	6th	105770.70705(54,94)	105770.7632(1)	0.05615(95)
		105770.69820(38,84)		

* obtained by including recalibrated infrared values from the work by Hernäng [41].

The re-evaluation has resulted in some revised hyperfine parameters (in cm^{-1}); the values from Ref. [1] are shown in italics for comparison:

State	A	B	^{83}Kr-^{86}Kr Isotope Shift
$5s'[^2P_{1/2}]$ $J=1$	−0.002467(1.5)**	−0.00372(10)**	−0.00456(25)
	−0.024678(55)	*−0.00387(32)*	*−0.00434*
$6s'[^2P_{1/2}]$ $J=1$	−0.0175277(840)	−0.000110(232)	−0.00937(31)
	−0.017405(96)	*−0.00023(55)*	*−0.00938*
$6s[^2P_{3/2}]$ $J=1$	−0.0047698(308)	−0.006209(332)	−0.00533(39)
	−0.004751(53)	*−0.00725(88)*	*−0.00512*
$7s[^2P_{3/2}]$ $J=1$	−0.0047381(548)	−0.006237(498)	−0.00885(28)
	−0.004622(45)	−0.00681(60)	−0.00907

** Values taken from Jackson [43].

Revised shifts of the even isotopes with respect to ^{86}Kr (in cm^{-1}); the values from Ref. [1] are shown in italics for comparison:

State	78–86	80–86	82–86	84–86
$7s[^2P_{3/2}]$ $J=1$	−0.02318(35)	−0.01709(30)	−0.01143(30)	−0.00555(30)
	−0.02304	*−0.01699*	*−0.01136*	*−0.00552*

0.01 cm^{-1} at 2500 nm. The primary data, however, are wavelengths in air. Neither the air pressure nor the temperature is given. Since most of the lines are also covered by the measurements in Ref. [5] we decided to recalibrate the wave numbers to ^{86}Kr by using the very accurate ^{86}Kr data from Ref. [5] as a reference. A perfect fit (standard deviation 0.010 cm^{-1}) could be achieved by applying the expressions for the refractive index of air published by Owens [42], by assuming dry air of 1013.25 mbar and by adjusting the temperature to 15.604 74 °C. This calibration (illustrated in Fig. 8) could be further improved by adding -0.0033 cm^{-1} $+0.024 \exp(-0.003\,75\,(\lambda_{air}[\mathrm{nm}]-1100\ \mathrm{nm}))$ to the data. From the four wavelengths in air, 1324.069 nm, 1383.288 nm, 1388.285 nm, and 1589.068 nm, we arrive at the following wave numbers for the $6s'$ state:

$$105\,146.384\,69\ \mathrm{cm}^{-1},\quad 105\,146.383\,00\ \mathrm{cm}^{-1},$$
$$105\,146.389\,35\ \mathrm{cm}^{-1},\quad 105\,146.411\,65\ \mathrm{cm}^{-1}.$$

The first three values look reasonable and an individual error of 0.010 cm^{-1} can be assumed. The fourth value shows by far the largest deviation for the entire table by Hernäng, containing about 100 wavelengths, and is, therefore, discarded. The offset of the average with respect to our measurement agrees with the other three differences shown in the final column of Table II within the error limit.

Table II also includes the revised hyperfine parameters. The changes mostly reflect the rescaling of the frequency intervals according to the changed distance between the neighboring iodine lines. In addition, a few measurements which yielded values deviating by more than three times the error limit have been discarded in the reanalysis. Since most scans were repeated many times this selection did not significantly reduce the information content. In the case of the $5s'$ state we calibrated the spectral data (in particular the free spectral range of the reference etalon) with the much more accurate values by Jackson [43] which are given in the table. The change in the isotope shifts for the even masses was

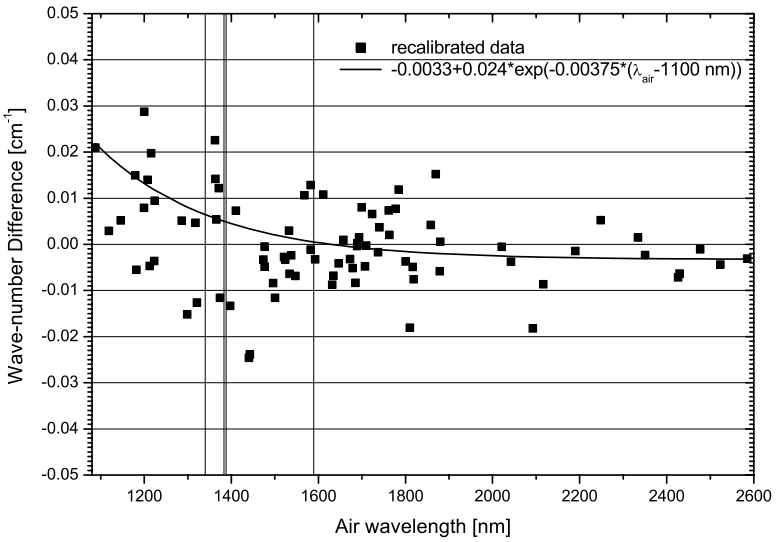

FIG. 8. Result of the recalibration of the infrared data by Hernäng [41] (see text); the vertical lines mark the positions of the four transitions of interest.

very small and was, therefore, evaluated only for the 7*s* case, where a pronounced deviation of the new iodine frequencies with respect to the iodine atlas had been found [1].

C. Estimate of the chirp-induced frequency shifts

In order to estimate the influence of the frequency chirp on the results we calculated the relative shift expected for the dyes used in our experiment. The basis of the calculation is the method described in Ref. [13]. The instantaneous frequency along the dye amplifier (z coordinate) is

$$f_{inst}(z,\tau) = f_{inst}(0,\tau) - \frac{\Delta\chi'(\omega)}{2\lambda n_s}\frac{d}{d\tau}\int_0^z N_e(z',\tau)dz',$$

$$\tau = t - n_S(\omega)\frac{z}{c}. \tag{1}$$

$\Delta\chi'(\omega)$ is the difference of the real parts of the excited-state (e) and ground-state (g) of the susceptibility, $\chi=\chi'+i\chi''$, n_s is the refractive index of the solvent, and N_e is the number density of the dye molecules in the excited state. The real part of the excited-state susceptibility is obtained from

$$\chi_e'(\omega) = 2\,\mathrm{P}\int_0^\infty \frac{\omega'\chi_e''(\omega')}{\pi(\omega'^2-\omega^2)}d\omega'$$

$$= -2cn_s(\omega)\,\mathrm{P}\int_0^\infty \frac{\sigma(\omega')}{\pi(\omega'^2-\omega^2)}d\omega', \tag{2}$$

P denoting the principal value, n_s the refractive index of the solvent, and σ stimulated-emission cross section. Since the energy stored in an amplifier is proportional to the gain coefficient [44] we approximate σ by the measured tuning curves to estimate the wavelength dependence of the frequency shift in arbitrary units. Assuming homogeneous pumping the amplifier cells we approximate the frequency variation of N_e also by that of σ. The temporal variation is averaged over the pulse for obtaining the mean frequency shift. We assume that the contribution from this time integral yields a rather constant scale factor just determined by the (highly symmetrical) pumping conditions and the gain depletion as a function of time which were similar under most of our conditions. Therefore, we evaluate the expression

$$\frac{\chi_e'(\omega)\sigma(\omega)}{\lambda},$$

neglecting the influence of χ'_g in $\Delta\chi'(\omega)$ [Eq. (1)].

The measured tuning curves were taken from Ref. [26]. The curves were normalized to the typical values achieved with fresh dyes, e.g., 130 mJ for Rhodamine 590. The tuning range was not fully determined in our measurements. In order to complete the curves we used the lengths of the tuning ranges from the Exciton product information sheets and linear interpolation.

The results for the three dyes used in our krypton experiment are shown in Fig. 9. The shifts for the four transition frequencies are marked with circles. Just the 6*s* shift is negative. It is interesting to note that the wave-number differences with respect to the values of Kaufman and Humphries [5] (Table II) qualitatively reproduce this behavior. The detailed sensitivity studies carried out for the I_2-based calibration show that these differences cannot be forced to coincide. It is, therefore, reasonable to ascribe the differences to chirp-induced shifts. The calibration of the chirp-induced shifts is achieved by fitting the expression

$$\Delta\nu_{\mathrm{KH,i}} = \Delta\nu_{\mathrm{KH,0}} + \alpha \mathrm{n_i}\delta_\mathrm{i}$$

to the three differences $\Delta\nu_{\mathrm{KH,i}}$ with respect to the results in Ref. [5]. n_i is the respective harmonic order and δ_i the theoretical shift determined from the analysis shown in Fig. 9 ($i\leqslant 3$). The two parameters $\Delta\nu_{\mathrm{KH,0}}$ and α were determined by a weighted least-squares fit. The result of this least-squares fit exceeds expections. The xuv frequency differences are reproduced to within 1.9 MHz ($5s'$), 0.6 MHz ($6s$), and 9.9 MHz ($7s$). The good agreement even for $7s$ is explained by the fact that the dye-laser frequency for the transition with the largest theoretical shift is multiplied by just a factor of 5 rather than 6 as in the case of the other two

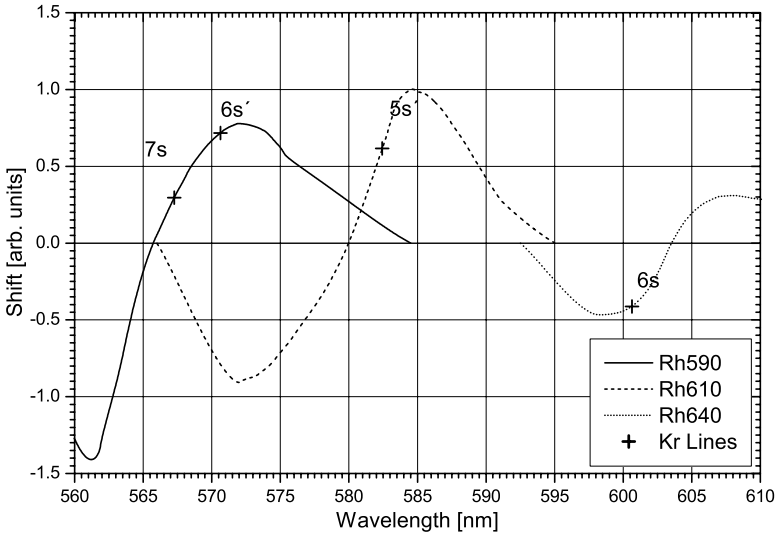

FIG. 9. Calculated tuning curves of the frequency shifts for the three dyes used in this experiment.

transitions. By introducing this calibration to Fig. 9 we obtain a maximum positive frequency shift for the visible dye laser of +5.0 MHz at 584.5 nm, and a maximum negative shift (561.2 nm) of −7.1 MHz. The positive limit is lower than the previously measured value of +9 MHz. A sensitivity analysis shows that the maximum values for the shift are certain to within ±2 MHz which, still, means lower values. However, we are not sure about potential frequency-cleaning effects in the generation of the higher harmonics, which could reduce the shifts.

The analysis yields a value of $-0.055\,530\ \mathrm{cm}^{-1}$ for $\Delta\nu_{\mathrm{KH},0}$ and $\alpha=-0.000\,166\,0\ \mathrm{cm}^{-1}$/(scale unit in Fig. 8). Due to the convincing analysis we assume an error of $0.0006\ \mathrm{cm}^{-1}$ for the frequency shift. $\Delta\nu_{\mathrm{KH},0}$ is rather close to the weighted average of the individual values, $-0.055\,71(46)\ \mathrm{cm}^{-1}$. It lies between the result of Ref. [3], $0.0558(13)\ \mathrm{cm}^{-1}$, and the high-precision value of $-0.055\,070(17)\ \mathrm{cm}^{-1}$, derived from the very recent publication by Witte *et al.* [45] brought to our attention shortly before finishing this paper. The mutual agreement between the three experiments excludes significant unidentified or not fully characterized errors and is encouraging for future precision xuv investigations.

The level of frequency chirping for our dye laser system is obviously rather low as compared with the results for the experiments listed in Table I and, in particular, the worst case of 100 MHz mentioned in the literature. The conditions of the experiments in Table I are rather different and mostly not favorable for avoiding chirp effects. The lowest frequency shifts are expected for side pumping a Bethune cell with a pump laser with a Gaussian or symmetrical time evolution and a homogeneous beam profile [13,14]. However, for the only experiment in Table I meeting these conditions an instantaneous frequency blueshift by more than 15 MHz is reported [13] which clearly exceeds the range of values obtained for our system. The surface area of the Bethune cells described in Ref. [13] is four times smaller than that of our cells which is, however, compensated by our four times higher pump pulse energy. Thus, it is difficult to find an explanation for this differing behavior.

V. CONCLUSIONS

Our 1987 measurements were carried almost with the maximum performance possible in a short, intense two-week effort. The high accuracy achieved in the revision of our data analysis nearly challenges that of the interferometrically determined longer-wavelength data of Ref. [5]. We quantitatively confirm the results published by Brandi *et al.* [3] which demonstrate the quality of both independent xuv experiments sharing just a single transition. Both xuv experiments yield frequencies consistently lower than that suggested by a recent presumably much more accurate UV two-photon experiment [45], although the differences stay within the error limits. In our experiment most of the small error contributions exhibit a tendency supporting slightly lower frequencies rather than the blueshift revealed by the comparison with Ref. [45]. The principal sources of uncertainty are the calibration procedure and the xuv generation. Brandi *et al.* are not fully explicit as to the potential influence of field-induced shifts [3,46,47].

The low frequency chirp observed for our system is a strong motivation for future improvements. Larger amplifier cells should be used in order to decrease the pump intensity. This is mandatory anyway because of the higher pump pulse energies available from state-of-the-art pump lasers. The most important improvement would be a substantial reduction of the laser bandwidth. A bandwidth reduction to less than 10 MHz and, thus, sub-MHz accuracies are feasible and would allow one to reduce the frequency chirp, to improve its control, and to reduce the need to apply chirp compensation techniques. From the very high ion yield of our 1987 experiment we conclude that a signal lowering even by several decades due to the expected reduced xuv intensity is acceptable. Many of the experimental parameters such as the efficiency of the grating, the beam overlap, and the ion transmittance of the mass spectrometer can be further optimized.

Future xuv experiments must be carried out with full control of all the three frequencies of interest, i.e., the continuous and pulsed output of the dye laser system and the xuv radiation. The two fundamental frequencies may be simultaneously monitored by Doppler-free methods or by laser-

induced fluorescence of a highly collimated effusive iodine beam, not possible in our case because we had to finish another, urgent experiment. It is strange enough that many later high-resolution experiments have not included a direct calibration of the pulsed output of the laser (iodine is almost ideal because of its small natural linewidth). Errors in the xuv part of the experiment may be minimized by varying the conditions in the xuv and ion sources.

Also a transition from dye lasers to solid-state lasers may help to improve the situation [48], although the operating wavelength are significantly longer requiring the generation of higher harmonics to reach the xuv region. On the other hand, very high pulse energies may be achieved by flashlamp pumping. 250 mJ of narrow-band radiation have recently been demonstrated in a Ti:sapphire laser system which, after solving some high-voltage problems caused by the high altitude of the laboratory (2674 m a.s.l.), is expected to yield 0.7 J [49].

With the arrival of short-pulse lasers with an ultrastable mode structure (frequency combs) new perspectives open up also for the xuv spectral region. The high-intensity frequency-comb lasers can be readily converted to very high harmonics [50]. After suitable amplification ultrahigh resolution experiments become feasible [51]. If the frequency combs are not distorted by the frequency conversion an unsurpassed accuracy may also be reached in the short-wavelength region. The capability of such experiments must be first tested with transitions known with sufficiently high accuracy such as those in the hydrogen atom. Also the krypton atom may, again, serve as a test case, at least at the accuracy level of ±3 MHz provided by the map of interferometrically determined level positions [5]. Intercomparisions at a higher accuracy level should also be made with narrow-band xuv laser sources, which means a major challenge for the development of such systems.

ACKNOWLEDGMENTS

The measurements underlying this paper were carried out when the authors were with the Department of Chemistry of the University of California (Berkeley) and the Materials and Chemical Sciences Division of the Lawrence Berkeley Laboratory. The experiment was supported by the Director, Office of Energy Research, Office of Basic Energy Sciences, Chemical Sciences Division of the U.S. Department of Energy under Contract No. DE-AC03-76SF00098. The authors thank E. Cromwell and M. Vrakking (who also critically read this manuscript) for their assistance in parts of the experiment, H. Knöckel and E. Tiemann for bringing their iodine computation program to their attention thus stimulating the revision of the Kr data, E. Saloman for his information on the infrared spectroscopy of krypton, W. Ubachs for providing some more details on the experiment in Ref. [3], as well as T. Udem for the hint on Ref. [45]. The authors also thank K. Boering, D. Newmark, and J. Stoner for their help in tracing the fate of the former Lee group archive containing the Kr spectra which, unfortunately, was not successful. We are further indebted to the extraordinary assistance by the machine shop of the UC Berkeley Chemistry Department.

[1] T. Trickl, M. J. J. Vrakking, E. Cromwell, Y. T. Lee, and A. H. Kung, Phys. Rev. A **39**, 2948 (1989).
[2] U. Hollenstein, H. Palm, and F. Merkt, Rev. Sci. Instrum. **71**, 4023 (2000).
[3] F. Brandi, W. Hogervorst, and W. Ubachs, J. Phys. B: At. Mol. Opt. Phys. **35**, 1071 (2002).
[4] J. Philip, J. P. Sprengers, P. Cacciani, C. A. de Lange, and W. Ubachs, Nucl. Phys. B **78**, 737 (2004).
[5] V. Kaufman and C. J. Humphreys, J. Opt. Soc. Am. **59**, 1614 (1969).
[6] V. Kaufman, J. Res. Natl. Inst. Stand. Technol. **98**, 717 (1993).
[7] S. Gerstenkorn and P. Luc, *Atlas du Spectre d'Absorption de la Molécule d'Iode entre 14 800–20 000 cm^{-1}* (Editions du CNRS, Paris, 1978).
[8] S. Gerstenkorn and P. Luc, Rev. Phys. Appl. **14**, 791 (1979).
[9] I. Velchev, R. van Dierendonk, W. Hogervorst, and W. Ubachs, J. Mol. Spectrosc. **187**, 21 (1998).
[10] S. C. Xu, R. van Dierendonk, W. Hogervorst, and W. Ubachs, J. Mol. Spectrosc. **201**, 256 (2000).
[11] C. Wieman and T. W. Hänsch, Phys. Rev. A **22**, 192 (1980).
[12] M. S. Fee, K. Danzmann, and S. Chu, Phys. Rev. A **45**, 4911 (1992).
[13] S. Gangopadhyay, N. Melikechi, and E. E. Eyler, J. Opt. Soc. Am. B **11**, 231 (1994).
[14] N. Melikechi, S. Gangopadhyay, and E. E. Eyler, J. Opt. Soc. Am. B **11**, 2402 (1994).
[15] I. Reinhard, M. Gabrysch, B. Fischer von Weikersthal, K. Jungmann, and G. zu Putlitz, Appl. Phys. B **63**, 467 (1996).
[16] K. S. E. Eikema, W. Ubachs, W. Vassen, and W. Hogervorst, Phys. Rev. A **55**, 1866 (1997).
[17] E. A. Hildum, U. Boesl, D. H. McIntyre, R. G. Beausoleil, and T. W. Hänsch, Phys. Rev. Lett. **56**, 576 (1986).
[18] K. Danzmann, M. S. Fee, and S. Chu, Phys. Rev. A **39**, 6072 (1989).
[19] E. E. Eyler, A. Yiannopoulou, S. Gangopadhyay, and N. Melikechi, Opt. Lett. **22**, 49 (1997).
[20] M. Niering, R. Holzwarth, J. Reichert, P. Pokasov, T. Udem, M. Weitz, T. W. Hänsch, P. Lemonde, G. Santarelli, M. Abgrall, P. Laurent, C. Salomon, and A. Clairon, Phys. Rev. Lett. **84**, 5296 (2000).
[21] J. R. M. Barr, J. M. Girkin, J. M. Tolchard, and A. I. Ferguson, Phys. Rev. Lett. **56**, 580 (1986).
[22] B. Bodermann, H. Knöckel, and E. Tiemann, Eur. Phys. J. D **19**, 31 (2002).
[23] H. Knöckel, B. Bodermann, and E. Tiemann, Eur. Phys. J. D **28**, 199 (2004).
[24] E. Cromwell, T. Trickl, Y. T. Lee, and A. H. Kung, Rev. Sci. Instrum. **60**, 2888 (1989).
[25] D. S. Bethune, Appl. Opt. **20**, 1897 (1981).

[26] E. F. Cromwell, Ph.D. Thesis, University of California, 1991 (unpublished).
[27] M. J. J. Vrakking, A. S. Bracker, T. Suzuki, and Y. T. Lee, Rev. Sci. Instrum. **64**, 645 (1993).
[28] R. H. Page, R. J. Larkin, A. H. Kung, Y. R. Shen, and Y. T. Lee, Rev. Sci. Instrum. **58**, 1616 (1987).
[29] D. Proch and T. Trickl, Rev. Sci. Instrum. **60**, 713 (1989).
[30] A. H. Kung, T. Trickl, N. A. Gershenfeld, and Y. T. Lee, Chem. Phys. Lett. **144**, 427 (1988).
[31] C. Y. Ng, B. H. Mahan, and Y. T. Lee, J. Chem. Phys. **65**, 1956 (1976).
[32] S. L. Anderson, F. A. Houle, D. Gerlich, and Y. T. Lee, J. Chem. Phys. **75**, 2153 (1981).
[33] V. I. Karataev, B. A. Mamyrin, and D. V. Shmikk, Sov. Phys. Tech. Phys. **16**, 1177 (1972); **41**, 1498 (1971)].
[34] B. A. Mamyrin, V. I. Karataev, D. V. Shmikk, and V. A. Zagulin, Sov. Phys. JETP **37**, 45 (1973); **64**, 82 (1973)].
[35] U. Boesl, H. J. Neusser, R. Weinkauf, and E. W. Schlag, J. Phys. Chem. **86**, 4857 (1982).
[36] A. Carrington, Proc. R. Soc. London, Ser. A **367**, 433 (1979).
[37] N. R. Daly, Rev. Sci. Instrum. **31**, 264 (1960).
[38] T. Trickl, E. F. Cromwell, Y. T. Lee, and A. H. Kung, J. Chem. Phys. **91**, 6006 (1989).
[39] D. R. Miller, in *Atomic and Molecular Beam Methods*, edited by G. Scoles (Oxford University Press, New York, 1988), Vol. 1, 721 pp.
[40] H. Haberland, U. Buck, and M. Tolle, Rev. Sci. Instrum. **56**, 1712 (1985).
[41] B. Hernäng, Ter Arkh. **33**, 471 (1966).
[42] J. C. Owens, Appl. Opt. **6**, 51 (1967).
[43] D. A. Jackson, J. Opt. Soc. Am. **67**, 1638 (1977).
[44] A. Siegman, *Lasers* (University Science Books, Mill Valley, California, 1986), 1283 pp.; see Eqs. (7.54) and (7.55) therein.
[45] S. Witte, R. T. Zinkstock, W. Ubachs, W. Hogervorst, and K. S. E. Eikema, Science **307**, 400 (2005).
[46] I. Velchev, W. Hogervorst, and W. Ubachs, J. Phys. B **32**, L511 (1999).
[47] F. Brandi, I. Velchev, W. Hogervorst, and W. Ubachs, Phys. Rev. A **64**, 032505 (2001).
[48] R. Seiler, T. Paul, M. Andrist, and F. Merkt, Rev. Sci. Instrum. **76**, 103103 (2005).
[49] T. Trickl and H. Vogelmann, *Reviewed and Revised Papers at the 23rd International Laser Radar Conference*, Nara (Japan), July 24 to 28, 2006, edited by C. Nagasawa and N. Sugimoto (Tokyo Metropolitan University, Tokyo, Japan, 2006) pp. 687–690.
[50] C. Gohle, T. Udem, M. Herrmann, J. Rauschenberger, R. Holzwarth, H. A. Schuessler, F. Krausz, and T. W. Hänsch, Nature (London) **436**, 234 (2005).
[51] R. T. Zinkstok, S. Witte, W. Ubachs, W. Hogervorst, and K. S. E. Eikema, Phys. Rev. A **73**, 061801(R) (2006).
[52] M. Vrakking (private communication).